J. Fluid Mech. (1970), *vol.* 42, *part* 4, *pp.* 671–687
Printed in Great Britain

A lock exchange flow

By I. R. WOOD
Water Research Laboratory, University of New South Wales, Australia

(Received 25 October 1968 and in revised form 19 August 1969)

In this paper the interchange flow between two reservoirs connected by a contraction and containing fluid of different densities is considered. The effect of the boundary layers on the floor and walls of the contraction on the depth of flow in the contraction is discussed for the case of single layer flowing from one reservoir to the other. Next the theory for a denser layer plunging under a stationary layer is developed. In this case there is a discontinuity at the point of intersection of the surfaces of the flowing and the stationary fluids and there are three possible flow régimes depending on whether this discontinuity occurs at, downstream of, or upstream of the contraction.

Finally, the case where there is an interchange flow with fluid flowing from each reservoir into the other is introduced. This latter theory parallels that developed by Wood (1968) for the case of two layers flowing from one reservoir through a contraction into another reservoir and as in this case there are two points of control, one at the position of minimum width and one (the virtual point of control) away from this position of minimum width.

Experiments are described for a single layer flowing through the contraction and the results of these are used to obtain an indication of the accuracy that could be expected from the experiments with the more complicated exchange flow. The experiments with the exchange flow verified the major elements of the theory.

1. Introduction

The flow of a heavy fluid under a lighter fluid is a relatively common natural occurrence. Indeed engineers since O'Brien & Cherno (1934) have been interested in the nature of the flow that arises when a lock gate with saline water on one side and fresh water on the other is opened and salt water intrudes under the fresh. This interest has continued up to the present day (Keulegan 1957; Barr 1963, 1967). The flow is normally studied in the laboratory in long flumes and in these cases the flow is unsteady. If, however, the lock gate connects two infinite reservoirs one containing saline water and the other containing fresh, and the gate is removed, then at a sufficient time after the removal of the gate the contraction controls the interchange flow and the flow is effectively steady. This type of flow is important in the interchange of salt and fresh water at the mouths of estuaries (Stommel & Farmer 1952, 1953). It would also occur when there is salt water under fresh water on one side of the lock gate and turbid water under fresh water on the other. These types of flow are illustrated in figure 1

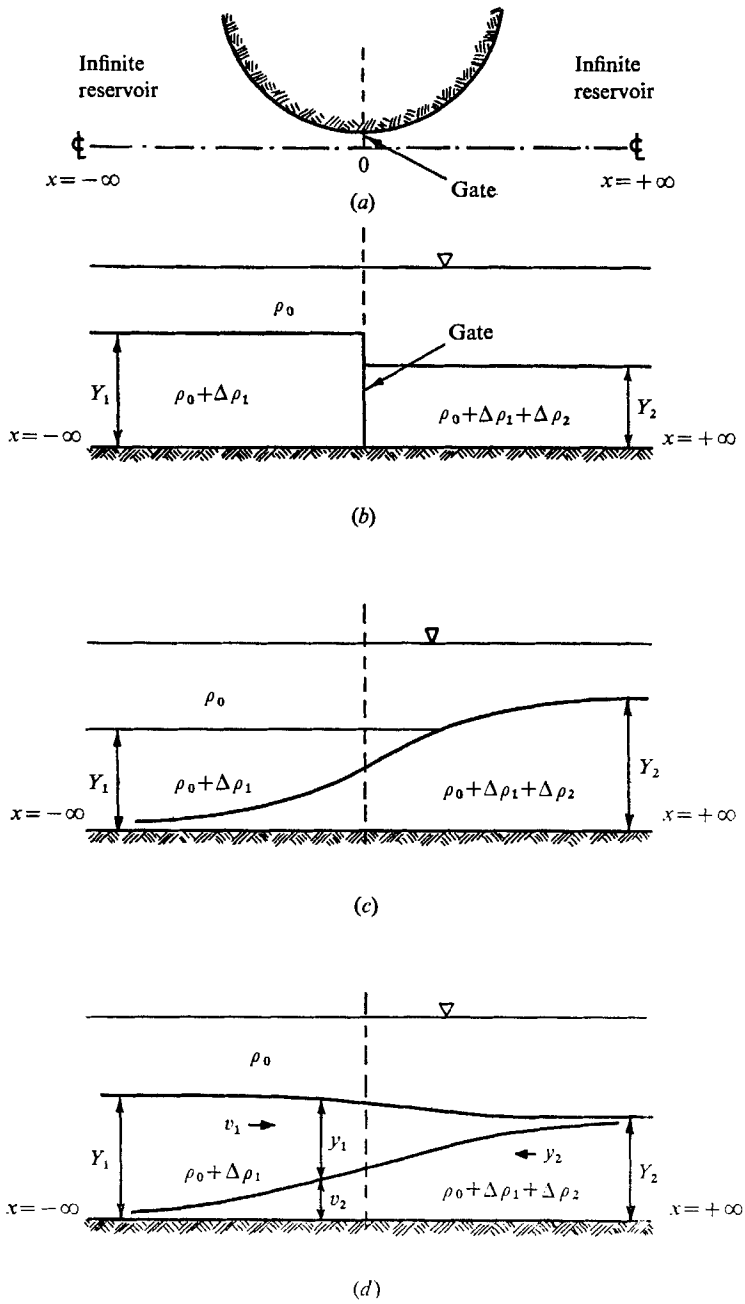

FIGURE 1. The types of exchange flow. (*a*) Plan. (*b*) Elevation, initial conditions $t = 0$. (*c*) Elevation, final conditions $t = \infty$, $Y_1 < Y_2$. (*d*) Elevation, final conditions $t = \infty$, $Y_1 > Y_2$.

and it is these flow situations that are being studied. The solutions obtained are those for the final steady flow of the lock exchange phenomena. However, the theory should be satisfactory in all cases where the reservoirs are large enough for the time for a particle to travel through the contraction to be short compared with the time for the streamline patterns to change due to the changes in levels in the reservoirs.

2. Theory

2.1. *The flow of a single layer*

Two reservoirs are connected by a channel of gradually varying width and the condition that the depth of the single flowing layer is continuously decreasing from the upstream to the downstream reservoir is examined. In the upstream reservoir the width becomes infinite, the velocity tends to zero and the surface approaches the still fluid level. In the downstream reservoir the width again becomes large and, because of limited flow through the contraction, the depth tends to a very small value.

In this section the flow of a real fluid is analyzed. This leads to an understanding of the magnitude of the errors involved in using the inviscid fluid assumption in the more complicated flows and is an aid in interpreting the experimental results.

Consider a contraction connected to an infinite reservoir as illustrated in figure 2. Let the density of the fluid in layers 0 and 1 be ρ_0 and $\rho_1 = \rho_0 + \Delta\rho_1$ and let the depth of layer 1 in the reservoir be Y_1. Further the width of the contraction is $b(x)$ where x is the distance measured along the contraction centreline. Let the discharge in the flowing layer be Q_1 and the depth of the layer at any position x be y_1. Suppose the velocity at a point in the region of flow is v and the area of flow A. Assume that the rate of convergence of the contraction is sufficiently small so that the vertical curvature of the streamlines is negligible and hence the hydrostatic approximation is reasonable (Henderson 1966).

In the flow of any real fluid a boundary layer will exist adjacent to the walls and the interfaces between the fluids. Because of the existence of these boundary layers the flow external to these layers is displaced and the appropriate displacement thickness of these boundary layers must be allowed for when comparing experiment and theory. In what follows the fluid will be considered as divided into a region where the flow has not been affected by the boundary layers against the walls, floor and interface, and a region within the boundary layer. This division is, however, not critical and should the boundary layers extend throughout the flow the argument is not affected.

Let V_I be the velocity calculated assuming the fluid is inviscid. (This will be the actual velocity in the region outside the boundary layers.) Then the effective area $\bar{A}$ at any section in the contraction may be calculated from

$$v_I \bar{A} = \int_A v dA = Q_1. \tag{1}$$

Further, at the mid-depth of the flow ($\frac{1}{2}y$) an effective width $\bar{b}$ may be calculated

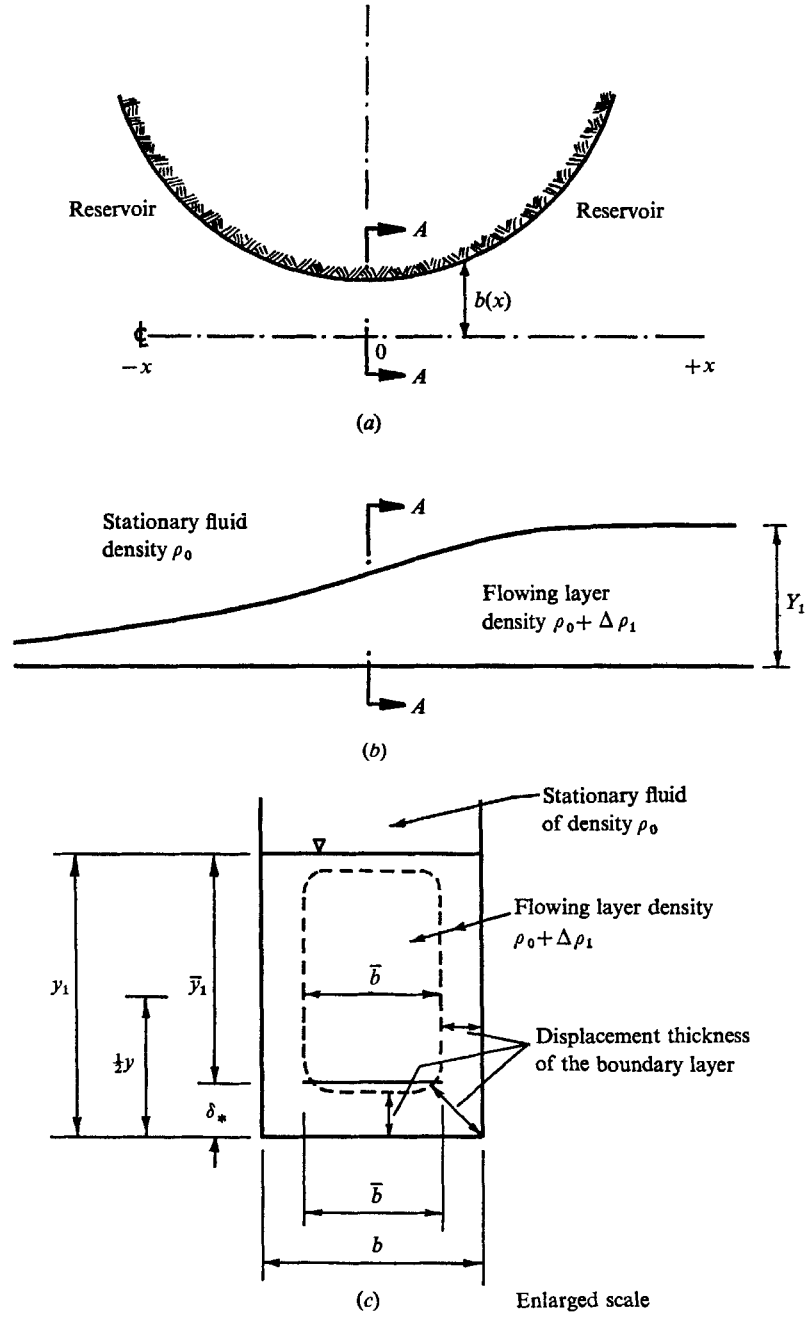

FIGURE 2. The details of a single flowing layer. (*a*) Plan. (*b*) Elevation. (*c*) Section AA of the elevation.

from
$$v_I \bar{b} = \int_0^b v db. \tag{2}$$

From these we define an average depth
$$\bar{y}_1 = \bar{A}/\bar{b}. \tag{3}$$

Combining the hydrostatic pressure and the potential energy terms, Bernoulli's equation in the region where the flow is not affected by viscosity is
$$\frac{1}{2}\frac{\rho_1 v_I^2}{\Delta\rho_1 g} + y_1 = Y_1, \tag{4}$$

or
$$\frac{1}{2}\frac{\rho_1}{\Delta\rho_1 g}\frac{Q_1^2}{\bar{b}_1^2 \bar{y}^2} + y_1 = Y_1. \tag{5}$$

If Q_1 is known and the conditions at infinity are known $(Y_1, \Delta\rho_1, \rho_1)$ then for the inviscid case where $\bar{y}_1 = y_1$ and $\bar{b} = b$ this equation yields y_1 in terms of the width b at every x. The remaining equation required to determine the value for Q_1 is obtained by assuming that the interface slopes smoothly from its value of Y_1 in the wide upstream reservoir to its very small value in the wide downstream reservoir (figure 2), and thus dy/dx at the position of minimum width is finite. For the case where the fluid is not inviscid the same method is used but a displacement thickness is defined as
$$\delta_* = y_1 - \bar{y}_1$$
and, using this expression, y_1 is eliminated from (5). Then differentiating (5) with respect to x we obtain
$$\frac{d\bar{y}_1}{dx}\left[1 - \frac{\rho_1}{\Delta\rho_1 g}\frac{Q_1^2}{\bar{b}^2\bar{y}^3}\right] + \frac{d\delta_*}{dx} - \frac{d\bar{b}}{dx}\frac{\rho_1 Q_1^2}{\Delta\rho_1 g \bar{y}_1^2 \bar{b}^3} = 0. \tag{6}$$

Now the growth of the boundary layer is small and $d\delta_*/dx$ may be neglected. Thus at the position where $d\bar{b}/dx$ equals zero for $d\bar{y}_1/dx$ to be finite we have
$$F_1^2 = \frac{\rho_1}{\Delta\rho_1 g}\frac{Q_1^2}{\bar{b}^2\bar{y}_1^3} = 1. \tag{7}$$

Substituting from (7) into (5) we obtain, at the position where $d\bar{b}/dx$ equals zero,
$$y_1/Y_1 = \tfrac{2}{3} + \tfrac{1}{3}\delta_*/Y_1. \tag{8}$$

Thus the boundary layers on the floor of the channel and between the flowing and stationary layers increase the depth at the minimum width by one third of the displacement thickness (δ_*). Further if the width through the contraction is very narrow the boundary layers on the wall of the contraction increase the effective displacement thickness (δ_*).

2.2. *The flow of multiple layers*

Having briefly outlined the effects of the viscous boundary layer in the most simple flow case we proceed assuming that the fluids are inviscid. Again the hydrostatic assumption is used and this limits the solution to gradual contractions. In this case three layers $(0, 1, 2)$ are considered with densities ρ_0,

$\rho_1 = \rho_0 + \Delta\rho_1$ and $\rho_2 = \rho_1 + \Delta\rho_1 + \Delta\rho_2$. The upper layer is considered as very deep and an interchange flow between layers (1) and (2) is considered. This type of flow may be produced in the laboratory by placing a submerged gate in a contraction connecting two reservoirs containing fresh water. Salt waters of different densities are then placed under the fresh water on either side of the gate (figure 1 (*b*)). Now provided the hydrostatic pressure from the denser layer at the base of the gate is greater than that of the lighter layer, then once the gate is removed an interchange flow of the type illustrated in figures 1 (*c*) or 1 (*d*) develops.

Let the lower two layers have depths in the wide reservoirs of Y_1 and Y_2. The geometry of the contraction is assumed to be the same as previously, and the discharges in the layers are taken as Q_1 and Q_2 respectively. Further, let the velocities and depths at any position in the final steady-state flow be v_1, v_2, y_1 and y_2 respectively. It is apparent that at the base of the gate the pressure from the denser fluid is greater than that from the lighter fluid if $Y_2(\Delta\rho_1 + \Delta\rho_2) > Y_1\Delta\rho_1$. If this is satisfied then the Bernoulli equations for the flowing layers are

$$\frac{1}{2}\frac{\rho_1}{\Delta\rho_1 g}\left(\frac{Q_1}{by_1}\right)^2 + y_1 + y_2 = Y_1, \tag{9}$$

$$\frac{1}{2}\frac{\rho_2}{\Delta\rho_2 g}\left(\frac{Q_2}{by_2}\right)^2 + \frac{\Delta\rho_1}{\Delta\rho_2}y_1 + \left(1 + \frac{\Delta\rho_1}{\Delta\rho_2}\right)y_2 = \left(1 + \frac{\Delta\rho_1}{\Delta\rho_2}\right)Y_2. \tag{10}$$

These two equations, together with the condition that dy_1/dx and dy_2/dx remain finite determine the final steady-state flow in case of figure 1 (*d*) and for most of the flow situations of the type illustrated in figure 1 (*c*). The exception is the case where the surfaces of the stationary layer (1) and the flowing layer (2) intersect at the point of the minimum width (i.e. where $db/dx = 0$).

(*a*) *The case of a single layer plunging under a stationary layer.* Consider firstly the case where $Y_1 < Y_2$. Here there is no flow in layer (1) (figure 1 (*c*)). In this case the form of the Bernoulli equation will be different in the regions upstream and downstream of the point where the flowing layer plunges under the stationary fluid. Three distinct flow régimes are possible, depending upon whether this plunge point is downstream of the position of minimum width (régime (1)), at the position of minimum width (régime (2)), or upstream of the position of minimum width (régime (3)).

Defining $\alpha_{12} = \Delta\rho_1/\Delta\rho_2$ the equation obtained from (10) for the region where $y_2 > Y_1$ (i.e. upstream of the point of intersection of the flowing and the stagnant fluid) is

$$\frac{1}{2}\frac{\rho_2}{\Delta\rho_2 g}\left(\frac{Q_2}{b}\right)^3 \frac{1}{Y_2^3} = (1 + \alpha_{12})\left(1 - \frac{y_2}{Y_2}\right)\left(\frac{y_2}{Y_2}\right)^2. \tag{11}$$

In the region where $y_2 < Y_1$ (i.e. downstream of the point of intersection of the surface of the flowing and the stagnant fluid) we obtain, after substituting in (10) from equation (9) with $Q_1 = 0$

$$\frac{1}{2}\frac{\rho_2}{\Delta\rho_2 g}\left(\frac{Q_2}{b}\right)^2 \frac{1}{Y_2^3} = \left[(1 + \alpha_{12})\left(1 - \frac{y_2}{Y_2}\right) - \alpha_{12}\left(\frac{Y_1}{Y_2} - \frac{y_2}{Y_2}\right)\right]\left[\frac{y_2}{Y_2}\right]^2. \tag{12}$$

These two equations are plotted in figure 3 for the case of $\alpha_{12} = 1$ with $(\rho_2/\Delta\rho_2 g)(Q_2/b)^2\, 1/Y_2^3$, a type of Froude number, as ordinate and y_2/Y_2 as abscissa. The

curve $OA'AM_1M_2BY_2$ is a plot of equation (11) and curves $OB'A$, $OC'M_2$, $OD'M_3B$ and $OE'M_4Y_2$ are plots of equation (12) for Y_1/Y_2 equalling 0·5, 0·80, 0·95 and 1·0 respectively. Consider now an example of the flow in each régime. The case where $Y_1 = 0{\cdot}5Y_2$ is an example of régime (1) where the plunge point occurs downstream of the position of minimum width. The complete solution for the value of $(\rho_2/\Delta\rho_2 g)\,(Q_2/b)^2 1/Y_2^3$ is given by $OB'AM_1M_2BY_2$. The segment of this curve $OB'A$ is a solution of equation (12) and the segment $AM_1M_2BY_2$ is a solution of (11). It is apparent that the maximum value of Q_2/b (i.e. the value at the position of minimum width) is unaffected by the downstream depth Y_1 and is determined from (11) as in §2.1. This maximum occurs when $y_2 = \frac{2}{3}Y_2$ and this condition implies that at the minimum width dy_2/dx is finite. At the junction of the two curves (i.e. where $y_2 = Y_1$) there is a discontinuity and this implies a discontinuity in dy_2/dx. In this case and indeed in the whole of régime (1) where $Y_1 < \frac{2}{3}Y_2$ the contraction controls the flow and discharge is the same as if there were no Y_1.

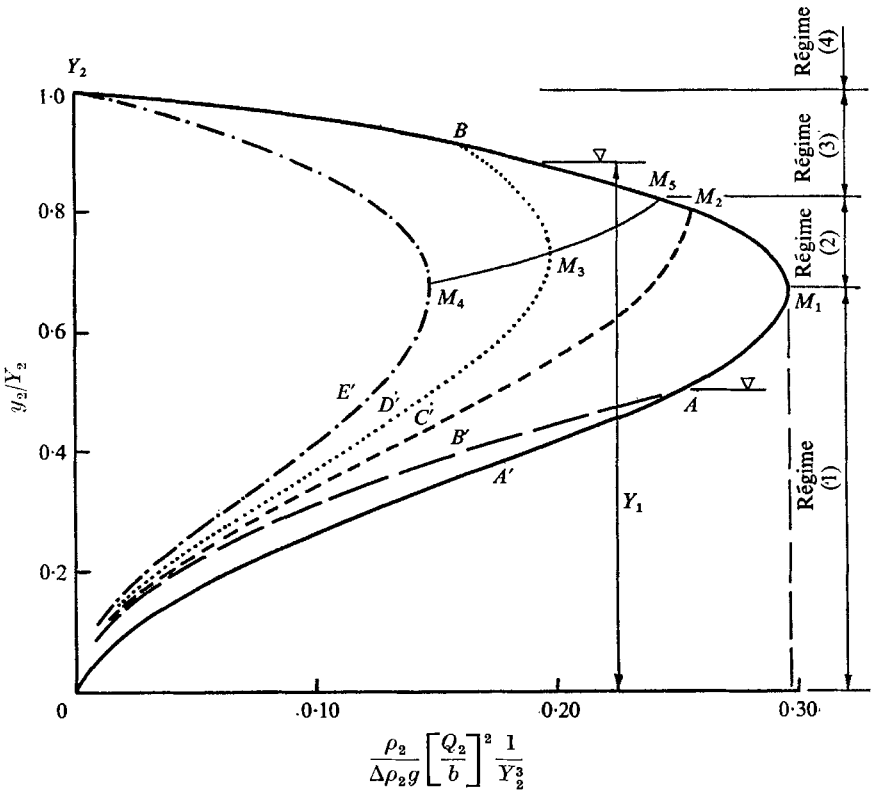

FIGURE 3. The solution for the plunging layer. The plot of the dimensionless depth (y_2/Y_2) *versus* a discharge parameter $(\rho_2/\Delta\rho_2 g)(Q_2/b)^2(1/Y_2^3)$. ——, equation (11). Equation (12): ——, $Y_1/Y_2 = 0{\cdot}5$; – – – –, $Y_1/Y_2 = 0{\cdot}666$; . . . . . , $Y_1/Y_2 = 0{\cdot}80$; —·—·—, $Y_1/Y_2 = 1{\cdot}00$.

Consider now the case where $Y_1 > \frac{2}{3}Y_2$. The curve $OC'M_2BY_2$ is an example of the type of flow in régime (2). In this case $OC'M_2$ is a solution of equation (12) and M_2BY_2 is a solution of equation (11). In this flow the maximum value of

Q_2/b (the value that will occur at the minimum width of the contraction) is obtained by the intersection of equations (11) and (12). At this point (the minimum width) there is a discontinuity in the slope of the curve of y_2/Y_2 *versus* $(\rho_2/\Delta\rho_2 g)\,(Q_2/b)^2\,1/Y_2^3$ and hence a discontinuity in dy_2/dx.

There are a range of flows that are possible where $Y_1 > \frac{2}{3}Y_2$ for which the maximum value of Q_2/b occurs where there is a sharp discontinuity in the curve of y_2/Y_2 *versus* $(\rho_2/\Delta\rho_2 g)\,(Q_2/b)^2\,1/Y_2^3$. For these cases there is a discontinuity in the effective Froude number of the flow. Upstream of the discontinuity the effective Froude number is $(\rho_2/[(\Delta\rho_1+\Delta\rho_2)g])\,(Q_2/by_2)^2\,1/y_2$ and the flow is subcritical. Downstream of the discontinuity the effective Froude number is $(\rho_2/\Delta\rho_2 g)\,(Q_2/by_2)^2\,1/y_2$ and the flow is supercritical. Thus as in the case of a normal open channel flow the flow upstream of the minimum width is subcritical and downstream of it is supercritical.

In régime (3) the plunge point is upstream of the position of minimum width and a typical curve is $OD'M_3BY_2$. The maximum value of Q_2/b is determined from (12). In this case the discontinuity in the curve of y_2/Y_2 *versus* $(\rho_2/\Delta\rho_2 g)\,(Q_2/b)^2\,1/Y_2^3$ has moved away from the maximum value of Q_2/b and thus at the position of minimum width dy_2/dx is again finite.

The maximum value of $(\rho_2/\Delta\rho_2 g)(Q_2/b)^2\,1/Y_2^3$ from equation (12) occurs when y_2/Y_2 equals $\frac{2}{3}[1+\alpha_{12}(1-Y_1/Y_2)]$ and is given by

$$\frac{\rho_2}{\Delta\rho_2 g}\left(\frac{Q_2}{b}\right)^2\frac{1}{Y_2^3} = 2\left[\tfrac{2}{3}+\tfrac{2}{3}\alpha_{12}\left(1-\frac{Y_1}{Y_2}\right)\right]^3. \tag{13}$$

The lower limit of régime (2) is $Y_1 = \frac{2}{3}Y_2$ and the upper limit is defined by the intersection of the equation (13) (curve $M_4M_3M_5$, figure 3), and equation (11). This is the solution of

$$\frac{\rho_2}{\Delta\rho_2 g}\left(\frac{Q_2}{b}\right)^2\frac{1}{Y_2^3} = 2(1+\alpha_{12})\left(1-\frac{y_2}{Y_2}\right)\left(\frac{y_2}{Y_2}\right)^2 = \left[\tfrac{2}{3}+\tfrac{2}{3}\alpha_{12}\left(1-\frac{Y_1}{Y_2}\right)\right]^3. \tag{14}$$

The value of y_2 obtained from the above defines the upper limit of region (2) (M_5, figure 3).

(*b*) *The interchange flow.* Now when $Y_1 > Y_2$ flow commences in the upper layer and we move into régime (4) where a slightly different approach is convenient. It is assumed that y_1 and y_2 decrease smoothly from their values in the upstream reservoirs (Y_1 and Y_2) to the value of zero in the infinitely wide downstream reservoirs. Thus the flow is as in figure 1(*d*) and providing the flow is stable it is appropriate to use the conditions that the values of dy_1/dx and dy_2/dx remain finite. The method then parallels that used by Wood (1968).

Defining $y_1' = y_1/Y_1$, $Y_2' = Y_2/Y_1$ and $y_2' = y_2/Y_1$ and substituting into equations (9) and (10) we get

$$\frac{1}{2}\frac{\rho_1}{\Delta\rho_1 g}\left(\frac{Q_1}{by_1}\right)^2\frac{1}{Y_1}+y_1'+y_2' = 1 \tag{15}$$

and

$$\frac{1}{2}\frac{\rho_2}{\Delta\rho_2 g}\left(\frac{Q_2}{by_2}\right)^2\frac{1}{Y_1}+\alpha_{12}y_1'+(1+\alpha_{12})y_2' = (1+\alpha_{12})Y_2'. \tag{16}$$

If Q_1 and Q_2 and the conditions at infinity Y_2' and α_{12} are known these two equations determine y_1', and y_2' in terms of b at every x. Two further equations

are required to solve for Q_1 and Q_2. These equations come from the condition that as b decreases from its large value at $x = +\infty$ through its minimum at $x = 0$ to a large value at $x = -\infty$ it is required that the lower layer continuously decreases from its value in the reservoir (Y_2') at $x = +\infty$ to a very small value at $x = -\infty$ and the upper layer continuously increases from a very small value at $x = +\infty$ to a value of Y_1 at $x = -\infty$. These conditions determine a possible flow. To obtain this flow it is necessary to obtain the conditions for which dy_1'/dx and dy_2'/dx are always finite.

Differentiating (15) and (16) with respect to x and solving for dy_1'/dx and dy_2'/dx we get

$$\frac{dy_1'}{dx} = \frac{1}{b}\frac{db}{dx}\frac{D_2}{D_1}, \tag{17}$$

$$\frac{dy_2'}{dx} = \frac{1}{b}\frac{db}{dx}\frac{D_3}{D_1}, \tag{18}$$

where

$$D_1 = (1-F_1^2)(1+\alpha_{12}-F_2^2)-\alpha_{12},$$

$$D_2 = F_1^2 y_1'[1+\alpha_{12}-F_2^2]-F_2^2 y_2',$$

$$D_3 = F_2^2 y_2'[1-F_1^2]-\alpha_{12}F_1^2 y_1',$$

and

$$F_1^2 = \frac{\rho_1}{\Delta\rho_1 g}\frac{Q_1^2}{b^2 y_1^3} \quad \text{and} \quad F_2^2 = \frac{\rho_2}{\Delta\rho_2 g}\frac{Q_2^2}{b^2 y_2^3}.$$

Now from equations (17) and (18) at the position of minimum width where $db/dx = 0$ we have dy_1'/dx and dy_2'/dx equal zero or $D_1 = 0$. We require the interfaces to be continuously sloping and can therefore exclude the case where the slopes are zero. Further, if at any other point $D_1 = 0$ then to obtain finite values of dy_1'/dx and dy_2'/dx then D_2 and D_3 must equal zero. It can be shown that the condition D_2 and D_3 equal zero together implies that D_1 also equals zero. It is these two conditions which ultimately enable the relationships between Q_1, Q_2, y_1' and y_2' to be obtained.

The condition that $D_1 = 0$ at the minimum width (where $db/dx = 0$) gives us three equations at this point. However, a fourth equation is required and it is therefore necessary to examine the variation of D_1 with x.

In the reservoir where $x = +\infty$, $y_2' = Y_2'$ and y_1' tends to a small value. Substituting these values into equations (15) and (16) we get after some algebra F_1^2 tends to a large value and F_2^2 tends to zero. Hence D_1 tends to a large negative value. Similarly when $x = -\infty$, D_1 tends to a large negative value. Three points of the curve of D_1 *versus* x (figure 4) have now been determined and it can be shown that when $b(x)$ has only one minimum the graph of D_1 *versus* x has only one turning point, and hence the possible curves of D_1 *versus* x are as in figure 4 and the equation

$$D_1 = 0 \tag{19}$$

holds at the position of minimum width and at some other point. This second point is called the point of virtual control (Wood 1968) and in order that dy_1'/dx and dy_2'/dx remain finite at this point then (from equations (17) and (18))

$$D_2 = 0 \tag{20}$$

and

$$D_3 = 0. \tag{21}$$

At this point of virtual control we have four equations, (20), (21), (15) and (16), and these may be solved for the four unknowns Q_1/by_1, Q_2/by_2, y_1' and y_2'. These equations are solved using $c^2 = \rho_2 v_2^2/\rho_1 v_1^2$, $\phi = \rho_1 v_1^2/2\Delta\rho_1 g Y_1$, y_1' and y_2' as the variables and eliminating y_1' and y_2' from (15) and (16) and substituting into (20) and (21). If A is defined as $Y_2'(1+\alpha_{12})-\alpha_{12}$ then the solutions are

$$c^2 = Y_2'(1+\alpha_{12})/\alpha_{12}, \tag{22}$$

$$\phi = \frac{A(1-A)}{2\alpha_{12}+3A-A^2}, \tag{23}$$

$$y_2' = \frac{2A(A+\alpha_{12})}{2\alpha_{12}+3A-A^2}, \tag{24}$$

$$y_1' = \frac{2(1-A)(A+\alpha_{12})}{2\alpha_{12}+3A-A^2}. \tag{25}$$

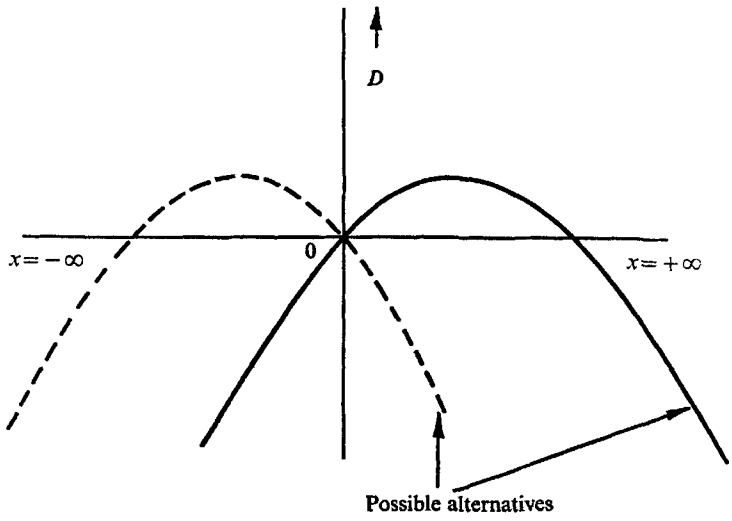

FIGURE 4. The variation of the determinant $D_1 = (1-F_1^2)(1+\alpha_{12}-F_2^2)-\alpha_{12}$ through the contraction. Note the point $x = 0$ is the position of minimum width in the contraction.

Equations (22), (24) and (25) lead to

$$\frac{\rho_2}{\rho_1}\left[\frac{Q_2}{Q_1}\right]^2 = \frac{Y_2'(1+\alpha_{12})}{\alpha_{12}}\left(\frac{A}{1-A}\right)^2. \tag{26}$$

This completes the calculations at the virtual control point and it is worth noting that calculations at this unknown point have given the ratio of discharges in the layers.

In obtaining the solution, the point of virtual control, Bernoulli's equations, and the conditions that the interfaces of the two flowing layers are continuous from one reservoir to the other have been used. Now Bernoulli's equation contains only the velocities squared. Hence the solutions at the virtual control do not depend on the direction of flow but only on the energy level of each layer in

the reservoir. Thus the solutions at this point are essentially the same as those obtained by Wood (1968).

It is now required to determine the conditions at the position of minimum width. Since the flow is steady the ratio of the discharges is independent of x and (26) must therefore hold at the position of minimum width. Further, since at the position of minimum width db/dx equals zero, (19) must be satisfied. These two equations together with (9) and (10) provide the solution for ϕ, c^2, y_1' and y_2'. Eliminating y_1' and y_2' from these equations we obtain from the expression for the discharge ratios (26)

$$\phi = \frac{(1+\alpha_{12})(c+Q_{21})Y_2' - c\alpha_{12} - (1+\alpha_{12})Q_{21}}{\alpha_{12}c^2(c+Q_{21}) - c\alpha_{12} - (1+\alpha_{12})Q_{21}}, \tag{27}$$

where $Q_{21} = Q_2/Q_1$. From $D_1 = 0$, (19), we obtain

$$(c-\phi[3c+2Q_{21}]) \cdot (Q_{21}(1+\alpha_{12}) - \phi[Q_{21}(1+\alpha_{12}) + \alpha_{12}(2c^3+2c^2Q_{21})]) - \alpha_{12}(1-\phi)^2 Q_{21} c = 0. \tag{28}$$

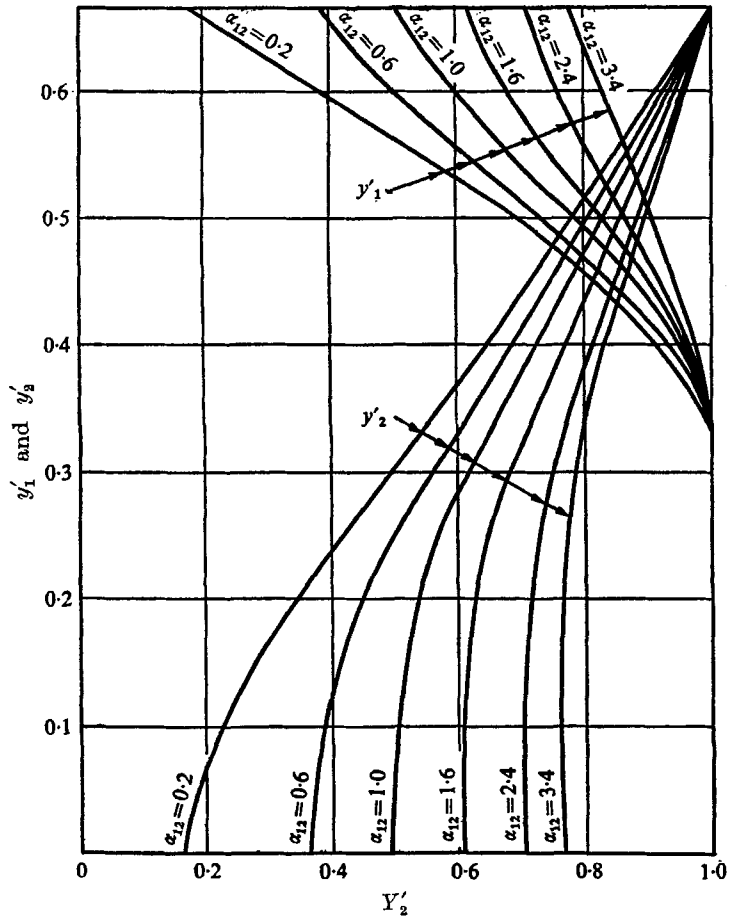

FIGURE 5. Computed values of the depth of the upper and lower layers (y_1' and y_2') at the minimum width of the contraction as a function of the ratio of the reservoir depths ($Y_2' = Y_1/Y_2$) for a range of density difference ratios (α_{12}).

The simultaneous solution of (27) and (28) was obtained using a computer which determined the values of ϕ, c, at the virtual control, calculated the gradient of D_1 at this virtual control, and then increased c until the second value at which $D_1 = 0$ was obtained. Once the value of c and ϕ at which $D_1 = 0$ was obtained the remaining variables at the minimum width were computed. Figure 5 gives the computed values of the depth of each layer (y_1' and y_2') obtained at the point of minimum width (the second position at which $D_1 = 0$) for the range of values of Y_2' and for constant values of α_{12}.

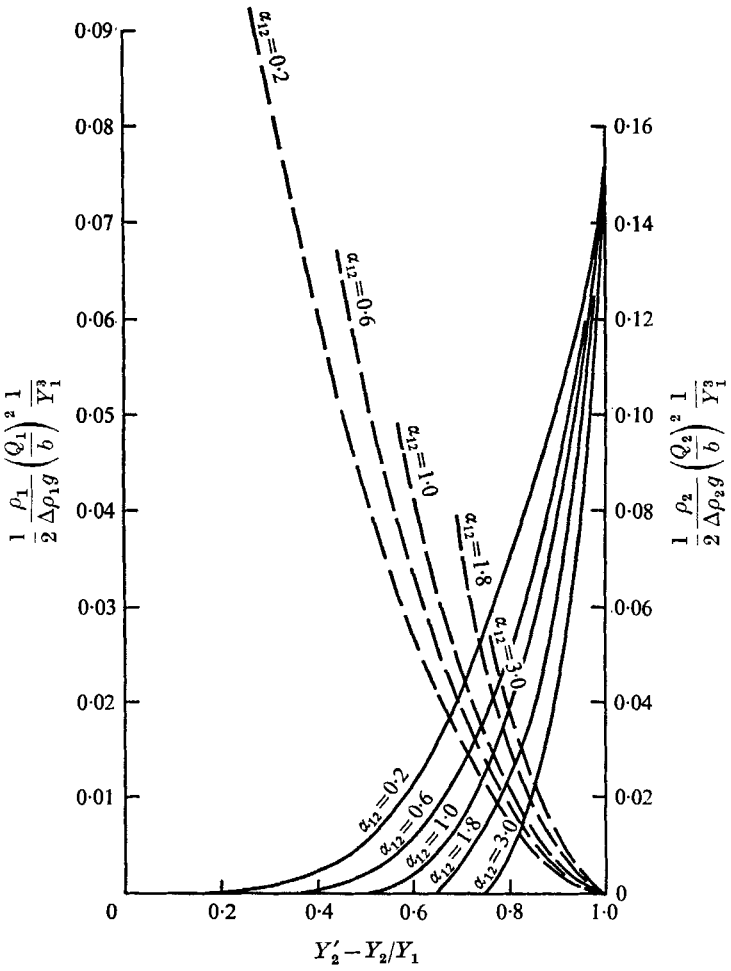

FIGURE 6. Computed values of a discharge parameter in each layer as a function of the ratio of the reservoir depths ($Y_2' = Y_1/Y_2$) for a range of density difference ratios (α_{12}). ———, $\frac{1}{2}(\rho_1/\Delta\rho_1 g)(Q_1/b)^2 1/Y_1^3$; ——, $\frac{1}{2}(\rho_2/\Delta\rho_2 g)(Q_2/b)^2 1/Y_1^3$.

Figure 6 gives the computed value of discharge parameters

$$\left[\frac{1}{2}\frac{\rho_1}{\Delta\rho_1 g}\left(\frac{Q_1}{b}\right)^2\frac{1}{Y_1^3} \quad \text{and} \quad \frac{1}{2}\frac{\rho_2}{\Delta\rho_2 g}\left(\frac{Q_2}{b}\right)^2\frac{1}{Y_1^3}\right]$$

for the range of values of Y_1' and constant values of α_{12}. From these curves the final steady-state properties of layers at the minimum width for given conditions in the reservoirs can be determined.

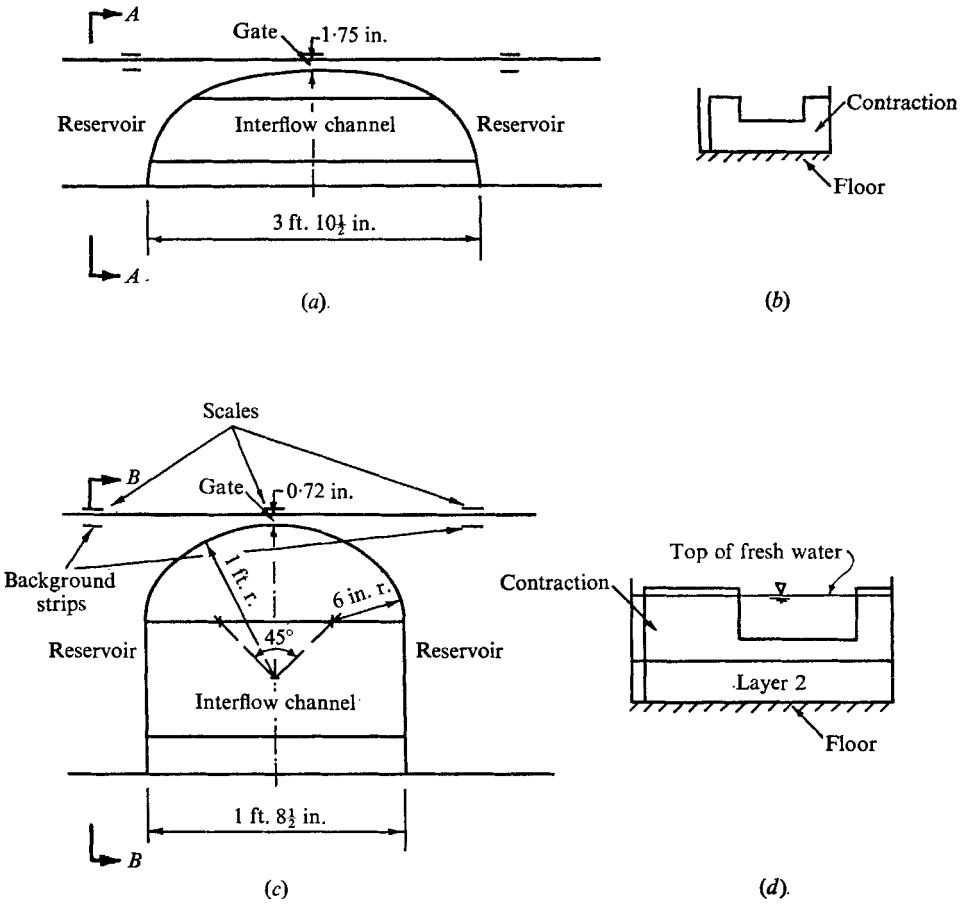

FIGURE 7. Details of the experimental contractions. (*a*) Plan. (*b*) Section *A*–*A*. (*c*) Plan. (*d*) Section *B*–*B*.

This theory has been developed by assuming that the slopes of the interfaces of the two flowing layers are continuous from reservoir to reservoir, but the results could have been obtained using long wave theory to determine the critical sections and carrying out the calculations at these sections. It is also important to note that although no Boussinesq type approximation has been used in the above theory the applicability of the results depends on the stability of interfaces and this will limit the use of the theory to cases where $\Delta\rho_1$ and $\Delta\rho_2$ are both small. This is discussed in the next section.

3. Experiments

Some experiments to confirm the major features of the analysis were carried out in a flume that was 8 ft. long, 2 ft. wide, and one foot high. The reservoirs were

formed by placing a contraction in the flume and the reservoirs were separated by a gate at the centre of the contraction. The geometry of the two contractions used is illustrated in figure 7. The flume was partially filled with fresh water and coloured salt waters of the different densities which made up layers (1) and (2) were pumped slowly under the fresh water. The experiments were commenced by removing the gate and, a short time after this, the flow settled down and the reservoir level changes became slow. A typical exchange flow experiment is illustrated in figure 8, plate 1. It is important to note that the velocities in the fresh water (ρ_0) were kept as low as possible by having a large interflow channel above the level of the flowing layers (figure 7).

The measurements in all experiments were recorded photographically. Initially black and white photographs were taken but light going through the dyed layers caused shadows on the contraction and made measurements difficult. This was overcome by using colour film. Scales were placed on the outer walls of the perspex flume at the centre of the contraction and in each reservoir (figure 7). White background strips were placed in each reservoir the same distance from the inner wall of the perspex flume as the white wall of the contraction (figure 7). Thus in every case when a scale was being read the observer was looking through the same distance of coloured fluid and the errors caused by any slight indistinctness of the interfaces should be constant.

In order that the theory should be strictly applicable to the experimental conditions it was necessary for the changes in the reservoirs to be slow and therefore the reservoirs large and the width of the contraction narrow. However, so that the one-dimensional approach used in the theory should be applicable the sides of the contraction had to converge and diverge gradually. Also, to minimize the effects of the boundary layers on the depth it was desirable to have large velocities through the contraction. This maximum velocity was limited by the necessity to maintain smooth stable interfaces. Indeed if the values of $\Delta\rho_1$ and $\Delta\rho_2$ used were too large the interfacial boundary layer remained very thin and instabilities of the type described by Thorpe (1968) developed. Further, to keep the boundary layers on the walls to a minimum it was desirable to have the contraction as wide as possible.

These requirements are conflicting and so to select a reasonable contraction some experiments were carried out with a single layer of water flowing under air through a contraction. Initially water was pumped into the reservoir upstream of the contraction and allowed to flow through the contraction. In this case for the contraction with a width of 1·75 in. (figure 7) the ratio of depth at the contraction to that far upstream was found to be $0{\cdot}68 \pm 0{\cdot}01$, and for the narrow contraction with a width of 0·72 in. this ratio was $0{\cdot}69 \pm 0{\cdot}01$. Two narrow contractions, one with a curvature considerably more gradual than the other were used. Both gave the value of the ratio as 0·69. The differences in the values obtained in wide and narrow contractions may have been caused by the increase in the effective displacement thickness of the floor boundary layer caused by the interference of the wall boundary layers (§2.1).

The narrow and the wide contractions were both used with a single layer of salt water flowing under fresh water. In every case the large interchange channel

provided above the level of the salt layers reduced the velocities in the fresh water to a small fraction of the velocities in the flowing salt layers. This was checked qualitatively in a number of experiments by the dropping of dye crystals in the flow and observing their subsequent traces. The values obtained for the wide contraction and narrow contraction were $0{\cdot}69 \pm 0{\cdot}01$ and $0{\cdot}71 \pm 0{\cdot}01$ respectively.

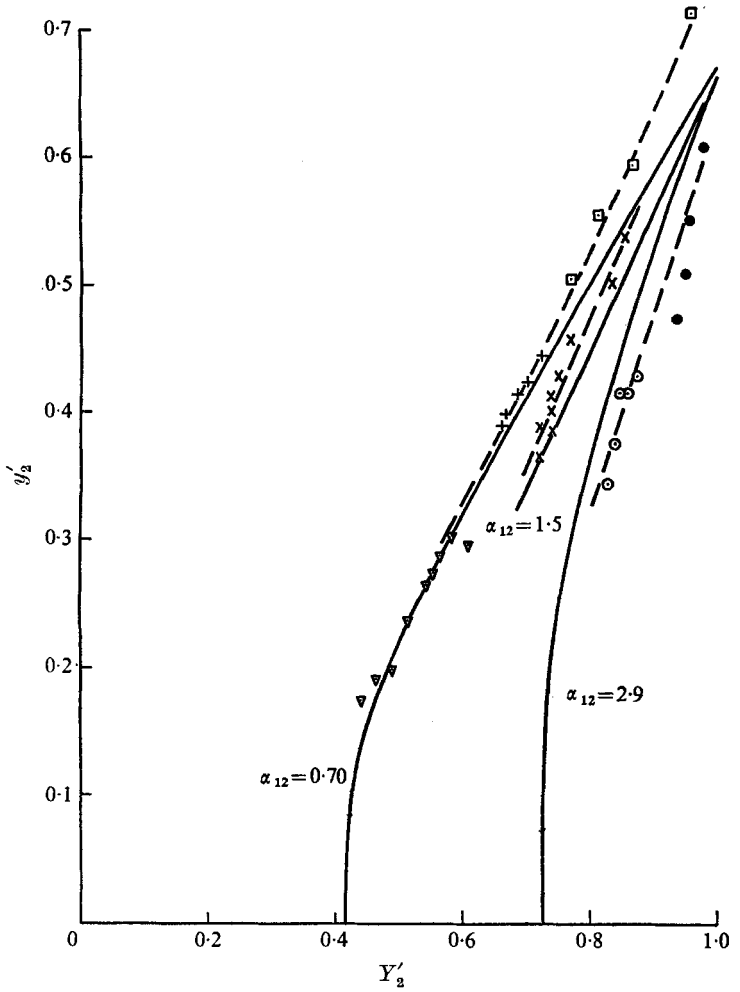

FIGURE 9. A comparison of the computed and experimental values of the depth of the lower layer (y_2') of a lock exchange flow. — —, y_2' experiment; ——, y_2' computed. Values of α_{12}: +, 0·685; □, 0·690; ▽, 0·622; ○, 3·1; ●, 2·7; ×, 1·5.

The differences between the case with an air–water interface and a salt–fresh water interface would be due to the appearance of a boundary layer and hence a displacement thickness on the salt–fresh-water interface and the increase in thickness of the displacement of the boundary layer on the floor. This latter effect would be caused by the lower Reynolds number of the flow.

These viscous effects would obviously affect the flows in the more complicated situations of lock exchange flow and thus great accuracy should not be expected

from the experiments. It was apparent that the wall effects would be the smallest, and the greatest accuracy could be expected from the wider contraction. However, it was found that the waves set up by the removal of the gate were more pronounced in this wide contraction and this made measurement in the more complicated flows difficult. It was therefore decided to use the narrow contraction and to accept the errors inherent in this geometry.

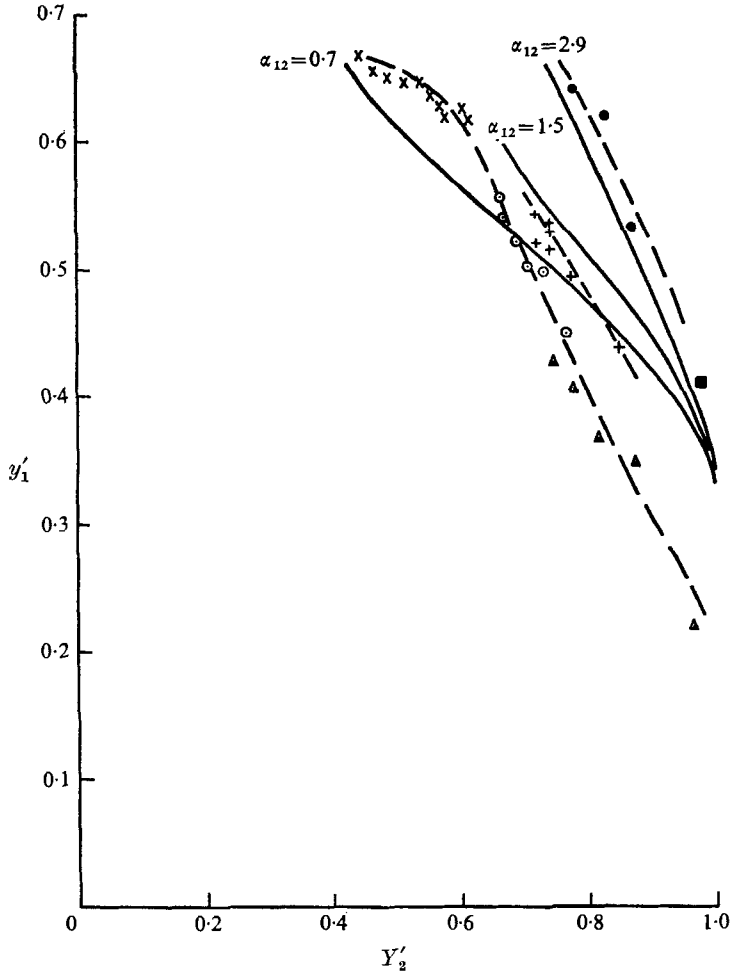

FIGURE 10. A comparison of the computed and experimental values of the depth of the upper layer (y_1') of a lock exchange flow. ——, y_1' experiment; ——, y_1' computed. Values of α_{12}: ○, 0·685; △, 0·690; ×, 0·622; ●, 3·1; ■, 2·7; +, 1·5.

The experiments with lock exchange flow were set up in a similar manner to those already described. Figure 8, plate 1, shows a typical exchange flow at a time when the changes in levels in the reservoirs were small. From this and similar photographs measurements were made of the levels of the interfaces of the layers.

In the theory it was assumed that the depth of y_1' in the reservoir containing ρ_2 and that of y_2' in the reservoir containing ρ_1 tended to zero. In the experiments

this was not the case and both y_1' and y_2' in their respective reservoirs tended to small finite values. In order to obtain the correct energy levels for layer (1) the effective Y_1 was the distance between the horizontal bed (the datum) and the upper interface and the effective Y_2 was the depth from the horizontal bed to the interface of layer (2) plus the effective head due to the upper fluid (i.e. $\Delta\rho_1 y_1/(\Delta\rho_1+\Delta\rho_2)$). All depths were expressed non-dimensionally in terms of Y_1.

Figures 9 and 10 show the experimentally determined curves and those obtained theoretically for α_{12} of 0·70, 1·5 and 2·9. The data exhibit the predicted variation with Y_2' and α_{12}. Indeed for the values of y_2' (figure 9) the theoretical and experimental curves agree to within the magnitude of the errors one might associate with the growth of boundary layers (6 %). However, the fact that two of the curves are above the theoretical curve and one is below is surprising. The agreement between the experimental and theoretical values of y_1' is not as good but it is only for the value $\alpha_{12} = 0{\cdot}65$ and Y_2' exceeding 0·80 that the agreement is outside the anticipated errors. In this region the small density differences and small depths in the upper layer (y_1) made the velocities extremely small and this could have made both the time-dependent and viscous effects important.

The work described in this paper forms part of a general investigation into the flow of multilayer systems of fluids and has in part been supported by a grant from the Australian Research Grants Committee. The author would like to thank those members of the Water Research Laboratory who assisted in making this investigation. Particular thanks are due to Mr P. Dind who assisted in carrying out the experimental programme.

REFERENCES

Barr, D. I. H. 1963 *La Houille Blanche*, **7**, 739.
Barr, D. I. H. 1967 *La Houille Blanche*, **6**, 619.
Henderson, F. M. 1966 *Open Channel Flow*. New York: Macmillan.
Keulegan, G. H. 1957 *U.S. Nat. Bur. Standards Rep.* no. 5186.
O'Brien, M. P. & Cherno, J. 1934 *Trans. Am. Soc. Civil Engrs.* **99**, 576.
Stommel, H. & Farmer, H. G. 1952 *J. Marine Res.* **11**, 205.
Stommel, H. & Farmer, H. G. 1953 *J. Marine Res.* **12**, 13.
Thorpe, S. 1968 *J. Fluid Mech.* **32**, 693.
Wood, I. R. 1968 *J. Fluid Mech.* **32**, 209.

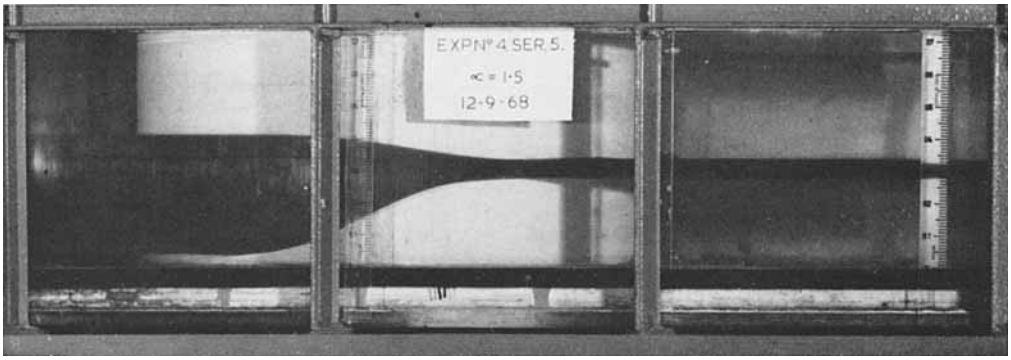

FIGURE 8. Photograph of a typical experiment.